Fast Hyperspectral Unmixing Using a Multiscale Sparse Regularization

Taner Ince, Nicolas Dobigeon

Fast Hyperspectral Unmixing Using a Multiscale Sparse Regularization

Taner Ince, *Member, IEEE*, Nicolas Dobigeon, *Senior Member, IEEE*

***Abstract*—This letter proposes a simple, fast yet efficient sparse hyperspectral unmixing algorithm. The proposed method consists of three main steps. First, a coarse approximation of the hyperspectral image is built using a off-the-shelf segmentation algorithm. Then, a low-resolution approximation of the abundance map is estimated by solving a weighted ℓ_1-regularized problem on this coarse approximation of the hyperspectral data. Finally, this low-resolution abundance map is subsequently used to design a sparsity-promoting penalization which acts as a spatial regularization informed by the coarse abundance map. It is incorporated into another weighted ℓ_1-regularized problem whose solution is a higher resolution abundance map. The computational efficiency of the two last steps is ensured by solving the two underlying optimization problems using an alternating direction method of multipliers. Extensive experiments conducted on simulated and real data show the effectiveness of the proposed method.**

***Index Terms*—Sparse unmixing, spatial regularization, total variation.**

I. Introduction

SPECTRAL unmixing (SU) aims at decomposing mixed pixels of hyperspectral images into pure spectral signatures characterizing the materials present in the scene (endmembers) and estimating their spatial distributions or relative proportions in each pixel (abundances) [1]. Even if light interactions occurring in the scene can suffer from multiple scattering effects [2], these interactions are often negligible [1], which eases the mathematical formulation of the hyperspectral unmixing [3] problem. Under this simplifying assumption, the measurements are described through the linear mixing model (LMM), i.e., resulting from linear combinations of the endmembers with weights defined by the abundances.

SU can be supervised or unsupervised according to the available knowledge about the endmembers. In an unsupervised context, the endmember spectral signatures should be extracted from the observed image or estimated jointly with the abundance maps [4]. Some examples of popular endmember extraction algorithms include vertex component analysis (VCA) [5] and N-FINDR [6]. Supervised unmixing algorithms rely on the availability of a predefined spectral library [7]. In this case, SU boils down to estimate the fractional abundance vectors. When the library is composed of a large number of spectral signatures, only a few of them are expected to contribute to the mixtures, i.e., most entries of the fractional abundance vector are expected to be zero. SU can then be formulated as a sparse regression task and, in this context, boils down to recovering sparse abundance vectors given an a priori known spectral library [1].

Sparse unmixing by variable splitting and augmented Lagrangian (SUnSAL) solves a constrained sparse regression problem by penalizing the ℓ_1-norm of the abundance vector. In a similar fashion, collaborative SUnSAL (CLSUnSAL) solves an $\ell_{2,1}$-norm regularized problem to promote the row-sparsity of abundance matrix since similar pixels are expected to share the same small set of endmembers. Although these sparsity-based unmixing methods performs, they rely on the spectral information only and ignore the spatial properties inherent to hyperspectral images.

Besides, exploiting the spatial characteristics of the image can be achieved by designing an appropriate regularization. Under a Bayesian formalism, abundance vectors are assigned Gaussian priors whose parameters define a Potts-Markov random field in [8]. Conversely, total variation (TV), defined as the 1st-order difference of neighboring abundances, is incorporated into SUnSAL-TV to promote spatially homogeneous (i.e., rather flat) abundance maps [9]. Double reweighted sparse regression and TV (DRSU-TV) enhances the sparsity of the abundance matrix by introducing spatial and spectral weights within the ℓ_1-norm penalization [10]. Following the success of TV-based unmixing methods, spectral-spatial weighted sparse unmixing (S^2WSU) combines the spatial and spectral properties into a single ℓ_1-regularizer which has a lower computational complexity compared to TV-based methods [11]. Another strategy to exploit the spatial correlations consists in investigating the linear independence of the neighboring pixels and enforcing the neighboring abundance vectors to obey a low-rank structure. Alternating direction sparse and low-rank unmixing (ADSpLRU) solves a sparsity regularized low-rank approximation by sliding a window on the hyperspectral data [12]. Finally, the authors of [13] adopts a two-phase iterative approach to capture the smoothness and preserve the discontinuity in abundance maps.

Despite the fact that TV-based regularization or low-rank approximations lead to reasonable unmixing results, they require to solve large scale optimization problems which come with high computational costs. Alternatively, multiscale methods have been advocated in several works to overcome the limitations inherent to TV and low-rank based methods

Part of this work has been supported by the ANR-3IA Artificial and Natural Intelligence Toulouse Institute (ANITI) under grant agreement ANITI ANR-19-PI3A-0004 and by the ANR IMAGIN project under grant agreement ANR-21-CE29-0007.

Taner Ince is with the Department of Electrical and Electronics Engineering, Gaziantep University, 27310 Gaziantep, Turkey (e-mail:tanerince@gantep.edu.tr).

Nicolas Dobigeon is with the University of Toulouse, IRIT/INP-ENSEEIHT, 31000 Toulouse, France, and also with the Institut Universitaire de France (IUF), France (e-mail: nicolas.dobigeon@enseeiht.fr).

Corresponding author: Taner Ince

[14], [15]. Multiscale sparse unmixing algorithm (MUA) decomposes the unmixing problem into two subproblems [16]. The first subproblem is solved in a transformed image domain while the second one is solved in the actual domain, which results in a low computational cost and favorable unmixing performance compared to TV-based methods. Following the idea of MUA, superpixel-based reweighted low-rank and total variation (SUSRLR-TV) performs a low-rank approximation for each region associated to superpixels and applies a TV criterion for the neighboring pixels [17]. SUSRLR-TV assumes that superpixels, which are known as homogeneous regions, should have a low-rank structure. SUSRLR-TV reaches good unmixing performance but comes with a high computational cost due to the TV term and several singular value decompositions required by the low-rank approximations.

To lighten the computational complexity without sacrificing the unmixing performance characterizing the spatially regularized algorithms, this paper proposes a fast sparse unmixing (FastUn) method exploiting a multiscale approach. The proposed method consists of two main steps. In the first one, a low resolution abundance map is obtained by transforming the original hyperspectral data into a lower dimensional space, following a strategy similar to MUA [16], which allows spatial and spectral properties to be jointly extracted from the image. However, contrary to MUA, the coarse abundance map estimated in this first step is subsequently resorted to design a spatial regularization incorporated into the second stage of the method. In this second step, the final high resolution abundance map is recovered by solving a weighted sparsity regularized minimization problem. This formulation has the great advantage of incorporating relevant spatial regularization into a computationally efficient unmixing algorithm.

The proposed method is described in Section II. Experimental results obtained on real and synthetic data sets are reported Section III. Section IV concludes the paper.

II. Fast sparse unmixing (FastUn)

As in most of the works dedicated to hyperspectral unmixing [1], the n measured pixel spectra gathered in the matrix $\mathbf{Y} \in \mathbb{R}^{L\times n}$ are assumed to result from the linear combinations of m elementary spectra (or endmembers), according to the linear mixing model

$$\mathbf{Y} = \mathbf{A}\mathbf{X} + \mathbf{N} \tag{1}$$

where $\mathbf{A} \in \mathbb{R}^{L\times m}$ is the spectral library composed of m endmembers, $\mathbf{X} \in \mathbb{R}^{m\times n}$ is the unknown abundance matrix to recover and $\mathbf{N} \in \mathbb{R}^{L\times n}$ stand for mismodeling effects and acquisition noise. The proposed method is composed of three main steps which consist in i) building a coarse approximation of the hyperspectral image ii) estimating the corresponding coarse approximation of the abundance map and iii) resorting to this coarse approximation to design a spatially-informed regularization used on the full resolution image. These three steps are described in what follows.

Coarse approximation of the hyperspectral image – To mimic TV-regularized unmixing method, the hyperspectral image $\mathbf{Y} = [\mathbf{y_1}, \ldots, \mathbf{y}_n]$ is segmented into $\bar{n} \in \mathbb{N}\backslash\{0\}$ homogeneous regions or superpixels. A coarse approximation $\bar{\mathbf{Y}} = [\bar{\mathbf{y}}_1, \ldots, \bar{\mathbf{y}}_{\bar{n}}] \in \mathbb{R}^{L\times\bar{n}}$ of this image is then computed by averaging the spectral signatures in each region. We denote $\mathcal{S}_i$ the set of pixel indexes defining the ith homogeneous region composed of $|\mathcal{S}_i|$ pixels, with $\mathcal{S}_i \cap \mathcal{S}_j = \emptyset$ $(i \neq j)$ and $\cup_{i=1}^{\bar{n}} \mathcal{S}_i = \{1, \ldots, n\}$. The ith superpixel of this approximation is defined as, for $i \in \{1, \ldots, n_c\}$,

$$\bar{\mathbf{y}}_i = \frac{1}{|\mathcal{S}_i|} \sum_{k\in\mathcal{S}_i} \mathbf{y}_k. \tag{2}$$

This averaging operation in each superpixel aims to reducing the original data into a lower dimensional space while capturing the spatial structure within the hyperspectral image.

In this work, the original hyperspectral image $\mathbf{Y}$ has been segmented using the simple linear iterative clustering (SLIC) algorithm [18]. This choice has been mainly motivated by the fact that SLIC is fast and requires a small set of parameters to be adjusted. Since it has been designed to segment grayscale or RGB images, a principal component analysis of the the hyperspectral image has been conducted and the the three first components are used to perform the segmentation.

Estimation of the coarse resolution abundance map – The coarse abundance map $\bar{\mathbf{X}} \in \mathbb{R}^{m\times\bar{n}}$ is obtained by unmixing the coarse approximation $\bar{\mathbf{Y}}$ of the hyperspectral image. In principle, any efficient yet fast unmixing algorithm could be used here. However, without loss of generality and to ensure consistency with the third and last step of the proposed pipeline, this coarse resolution unmixing is conducted by solving the reweighted sparsity-regularized problem

$$\min_{\mathbf{X}} \frac{1}{2}\|\bar{\mathbf{Y}} - \mathbf{A}\mathbf{X}\|_{\mathrm{F}}^2 + \bar{\lambda}\|\mathbf{W}\odot\mathbf{X}\|_1 + \iota_+(\mathbf{X}) \tag{3}$$

where $\iota_+(\cdot)$ is the indicator function on the positive orthant imposing the nonnegativity constraint, $\bar{\lambda}$ is a parameter adjusting the regularization, $\mathbf{W}$ is a weighting term which evolves at each iteration based on a rule to enhance the sparsity of the solution and $\odot$ denotes the term-wise product. The sparsity of the solution is enhanced by adjusting $\mathbf{W}$ inversely proportional to the estimated solution at each iteration (see details in Algo. 1). The problem (3) is separable and can be solved efficiently using an alternating direction method of multipliers (ADMM). More precisely, after introducing two auxiliary variables, the splitting scheme leads to the equivalent problem

$$\begin{aligned}\min_{\mathbf{X},\mathbf{V}_1,\mathbf{V}_2} \frac{1}{2}\|\bar{\mathbf{Y}} - \mathbf{A}\mathbf{X}\|_{\mathrm{F}}^2 + \bar{\lambda}\|\mathbf{W}\odot\mathbf{V}_1\|_1 + \iota_+(\mathbf{V}_2) \\ \text{s.t.} \quad \mathbf{V}_1 = \mathbf{X} \text{ and } \mathbf{V}_2 = \mathbf{X}.\end{aligned} \tag{4}$$

This problem can be solved following an algorithmic scheme similar to SUnSAL [19] with slight modifications induced by the weighting term. It is summarized in Algorithm 1. In this pseudo-code, the operators abs$(\cdot)$, soft$(\cdot)$ and max$(\cdot)$ as well as the inversion $\cdot^{-1}$ should be understood as component-wise. Moreover, the soft-thresholding operator in line 5 of Algo. 1 is defined as $\mathrm{soft}(t,\delta) = \mathrm{sign}(t)\max\{|t| - \delta, 0\}$.

Algorithm 1 Estimation of the coarse abundance map

Input: $\bar{\mathbf{Y}}$, $\mathbf{A}$, $\bar{\lambda}$, $\mu > 0$, ϵ,
Initialization: $k = 0$, $\mathbf{V}_1^{(0)}$, $\mathbf{V}_2^{(0)}$, $\mathbf{D}_1^{(0)}$, $\mathbf{D}_2^{(0)}$
$\mathbf{\Lambda} = \mathbf{A}^T\mathbf{A} + 2\mu\mathbf{I}$
while not converged **do**
  $\mathbf{X}^{(k+1)} = \mathbf{\Lambda}^{-1}(\mathbf{A}^T\bar{\mathbf{Y}} + \mu(\mathbf{V}_1^{(k)} + \mathbf{V}_2^{(k)} + \mathbf{D}_1^{(k)} + \mathbf{D}_2^{(k)}))$
  $\mathbf{W} = [\text{abs}(\mathbf{X}^{(k+1)} - \mathbf{D}_1^{(k)}) + \epsilon]^{-1}$
  $\mathbf{V}_1^{(k+1)} = \text{soft}(\mathbf{X}^{(k+1)} - \mathbf{D}_1^{(k)}, (\bar{\lambda}/\mu)\mathbf{W})$
  $\mathbf{V}_2^{(k+1)} = \max(\mathbf{0}, \mathbf{X}^{(k+1)} - \mathbf{D}_2^{(k)})$
  $\mathbf{D}_1^{(k+1)} = \mathbf{D}_1^{(k)} - (\mathbf{X}^{(k+1)} - \mathbf{V}_1^{(k+1)})$
  $\mathbf{D}_2^{(k+1)} = \mathbf{D}_2^{(k)} - (\mathbf{X}^{(k+1)} - \mathbf{V}_2^{(k+1)})$
  $k \leftarrow k + 1$
end while
Output: $\bar{\mathbf{X}} = \mathbf{X}^{(k)}$

Estimation of the full resolution abundance map – Given the coarse approximation $\bar{\mathbf{X}}$ of the abundance map, a crude estimation $\check{\mathbf{X}} = [\check{\mathbf{x}}_1, \ldots, \check{\mathbf{x}}_n] \in \mathbb{R}^{m\times n}$ of the full resolution abundance map can be obtained by assigning the abundance value $\bar{\mathbf{x}}_i$ estimated at the ith superpixel ($i = 1, \ldots, \bar{n}$) to the $|\mathcal{S}_i|$ pixels which composes it, i.e.,

$$\forall i \in \{1, \ldots, \bar{n}\},\ \forall k \in \mathcal{S}_i,\ \check{\mathbf{x}}_k = \bar{\mathbf{x}}_i \tag{5}$$

Since the coarse abundance map is expected to capture the inter-pixel spatial structure within each superpixel, this map is used to design a spatial weighting matrix to define a sparse regularization that can be interpreted as a proxy of TV. The ith column of the weighting matrix $\mathbf{S} = [\mathbf{s}_1, \ldots, \mathbf{s}_n] \in \mathbb{R}^{m\times n}$ is defined as ($i = 1, \ldots, n$)

$$\mathbf{s}_i = \left[\frac{1}{\|\check{\mathbf{X}}_{1,:}\|_2 + \epsilon}, \ldots, \frac{1}{\|\check{\mathbf{X}}_{m,:}\|_2 + \epsilon}\right]^T \tag{6}$$

where $\check{\mathbf{X}}_{j,:}$ denotes the jth row of $\check{\mathbf{X}}$ and $\epsilon > 0$ is a small constant to avoid numerical instabilities. Then the high resolution abundance map $\hat{\mathbf{X}}$ is then defined as the solution of the following weighted sparsity-regularized problem

$$\min_{\mathbf{X}} \frac{1}{2}\|\mathbf{Y} - \mathbf{A}\mathbf{X}\|_{\text{F}}^2 + \lambda\|\mathbf{S} \odot (\mathbf{X} - \check{\mathbf{X}})\|_1 + \iota_+(\mathbf{X}). \tag{7}$$

The proposed regularization aims at minimizing the difference between the low and high resolution abundance map to mimic 1st-order difference as in TV. However, it is known that TV blurs the edge details in the abundance map, we introduce a weight term to take into account the edge details. The weighting matrix $\mathbf{S}$ penalizes large differences between the low and high resolution maps to reduce any smoothing effect in the high resolution approximation. The problem (7) can be solved following an ADMM similar to Algo. 1. By introducing a pair of auxiliary variables, the problem can be rewritten as

$$\begin{aligned}\min_{\mathbf{X},\mathbf{V}_1,\mathbf{V}_2} \frac{1}{2}\|\mathbf{Y} - \mathbf{A}\mathbf{X}\|_{\text{F}}^2 + \lambda\|\mathbf{S} \odot \mathbf{V}_1\|_1 + \iota_+(\mathbf{V}_2) \\ \text{s.t.} \quad \mathbf{V}_1 = \mathbf{X} - \check{\mathbf{X}}; \quad \mathbf{V}_2 = \mathbf{X}.\end{aligned} \tag{8}$$

Algo. 2 details the steps followed to solve this problem.

In term of computational complexity, the proposed FastUn method is composed of Algo. 1 and Algo. 2. Since Algo. 1 is applied to a coarse approximation of the hyperspectral data (i.e., with $\bar{n} \ll n$), Algo. 2 dominates the computational complexity of FastUn where the term in step 1 can be precomputed. Therefore, the overall computational complexity is $\mathcal{O}(nmL)$ per iteration. It is worth noting that the complexity of FastUn is the same as SUnSAL which only solves a sparsity regularized unmixing problem without spatial regularization. Algo.'s 1 and 2 stop once reconstruction error reaches 10^{-6} or iteration number is 1000.

Algorithm 2 Estimation of the full resolution abundance map

Input: $\mathbf{Y}$, $\mathbf{A}$, $\mathbf{S}$, λ, $\mu > 0$, ϵ
Initialization: $k = 0$, $\mathbf{V}_1^{(0)}$, $\mathbf{V}_2^{(0)}$, $\mathbf{D}_1^{(0)}$, $\mathbf{D}_2^{(0)}$
$\mathbf{\Lambda} = \mathbf{A}^T\mathbf{A} + 2\mu\mathbf{I}$
while not converged **do**
  $\mathbf{X}^{(k+1)} = \mathbf{\Lambda}^{-1}(\mathbf{A}^T\mathbf{Y} + \mu(\mathbf{V}_1^{(k)} + \mathbf{V}_2^{(k)} + \mathbf{D}_1^{(k)} + \mathbf{D}_2^{(k)}))$
  $\mathbf{V}_1^{(k+1)} = \text{soft}(\mathbf{X}^{(k+1)} - \check{\mathbf{X}} - \mathbf{D}_1^{(k)}, (\lambda/\mu)\mathbf{S})$
  $\mathbf{V}_2^{(k+1)} = \max(\mathbf{0}, \mathbf{X}^{(k+1)} - \mathbf{D}_2^{(k)})$
  $\mathbf{D}_1^{(k+1)} = \mathbf{D}_1^{(k)} - (\mathbf{X}^{(k+1)} - \check{\mathbf{X}} - \mathbf{V}_1^{(k+1)})$
  $\mathbf{D}_2^{(k+1)} = \mathbf{D}_2^{(k)} - (\mathbf{X}^{(k+1)} - \mathbf{V}_2^{(k+1)})$
  $k \leftarrow k + 1$
end while
Output: $\hat{\mathbf{X}} = \mathbf{X}^{(k)}$

III. Experimental results

A. Simulated data sets

The proposed FastUn algorithm is compared with state-of-art TV-based and competitive multiscale based unmixing algorithms: SUnSAL-TV [9], S^{2}WSU [11], MUA [16], SUSRLR-TV [17], DRSUTV [10] and RDRSU [20]. These algorithms are quantitatively compared in term of signal reconstruction error (SRE) defined as $\text{SRE} = 10\log_{10}\frac{\|\mathbf{X}\|_{\text{F}}^2}{\|\mathbf{X}-\hat{\mathbf{X}}\|_{\text{F}}^2}$. The level ρ of sparsity of the solution is also monitored. They are defined as the proportion of elements in $\hat{\mathbf{X}}$ that are larger than a given threshold set as 5.0×10^{-3}.

Two simulated data sets have been considered. For both experiments, the pixel spectra have been generated according to the LMM (1). The endmember matrix $\mathbf{A}$ has been defined by extracting $m = 240$ signatures from the spectral library splib06 [21] which covers $L = 224$ spectral bands ranging from 0.4 to 2.5μm. The two simulated data sets, referred to as SD1 and SD2, differ by the generation of the true abundance map $\mathbf{X}$. For SD1, which consists of 75×75 pixels organized with squared patches, the abundance map has been generated by selecting 5 active endmembers out of the $m = 240$, i.e., with 5 non-zeros abundance values in each pixel. The abundance map associated to SD2, of spatial size 100×100 with a more realistic spatial organization, has been generated by selecting 9 endmembers from $\mathbf{A}$. The resulting linear mixtures have been corrupted by an additive Gaussian noise with different signal-to-noise ratios (SNR): SNR$\in \{20\text{dB}, 30\text{dB}, 40\text{dB}\}$. The regularization parameters of all algorithms have been adjusted using a grid search approach to reach the highest SRE. For RDRSU, MUA and SUSRLR-TV, the segmentation algorithm has been chosen as SLIC

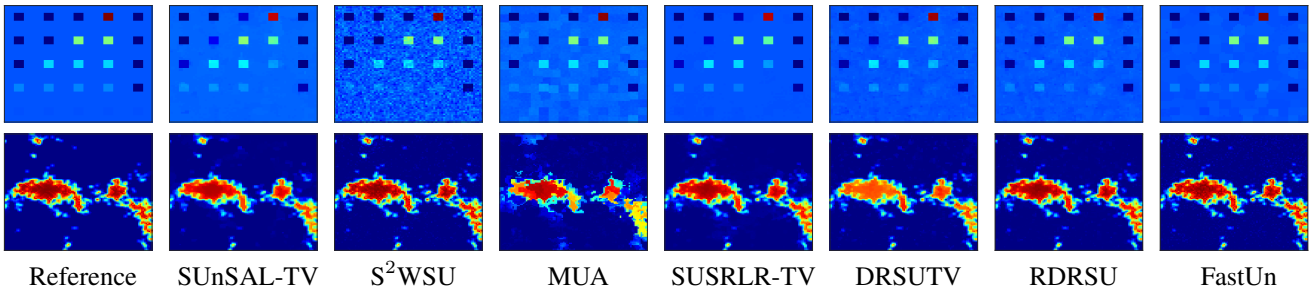

Fig. 1. Estimated abundance maps for endmember #4 in SD1 (top) and endmember #9 in SD2 (bottom) with SNR= 30dB.

TABLE I
SIMULATED DATA SETS: SRE AND SPARSITY LEVELS OBTAINED BY THE COMPARED ALGORITHMS.

			SUnSAL TV	S^{2}WSU	MUA	SUSRLR TV	DRSU TV	RDRSU	FastUn
SD1	20dB	**SRE**	7.06	5.28	7.68	14.83	6.46	20.48	**21.62**
		sparsity	0.0902	0.0270	0.0543	0.0357	0.044	0.00211	**0.0203**
	30dB	**SRE**	13.34	15.11	14.96	23.35	23.61	27.95	**29.25**
		sparsity	0.0388	0.0240	0.0401	0.0211	0.0246	0.0204	**0.0200**
	40dB	**SRE**	21.48	26.40	23.74	37.29	36.45	35.00	**37.68**
		sparsity	0.0258	0.0200	0.0264	0.0201	0.02	0.020	**0.0199**
SD2	20dB	**SRE**	6.25	6.61	6.74	7.56	6.73	**13.29**	12.27
		sparsity	0.0900	0.0379	0.0745	0.0670	0.0482	**0.0229**	0.0230
	30dB	**SRE**	11.16	9.62	8.22	12.01	13.74	19.00	**19.63**
		sparsity	0.0501	0.0179	0.0658	0.0323	0.0281	0.0197	**0.0174**
	40dB	**SRE**	17.26	31.11	11.47	21.11	18.01	**28.66**	28.57
		sparsity	0.041	0.0136	0.0561	0.0017	0.0178	0.0144	**0.0144**

whose parameters have been set as prescribed in their original papers. For the FastUn algorithm applied to SD1 (resp. SD2), the SLIC parameter has been set to 8, 6 and 6 (resp. 7, 6 and 6) for the noise levels SNR= 20dB, 30dB and 40dB.

The SRE and the sparsity levels reached by all algorithms for SD1 and SD2 are reported in Table I where the best scores are highlighted with bold face. FastUn generally provides the best results for the two data sets for all noise levels except for the data sets SD2 with SNR= 20dB or SNR= 40dB for which RDRSU provides slightly better results. For the lowest SNR case, this can be explained by the inaccurate segmentation, leading to a weighting matrix $\mathbf{S}$ that does not encode properly the spatial information. Fig. 1 shows the estimated abundance maps for two particular endmembers of SD1 and SD2 for a noise level of SNR= 30dB. Visually, it appears that FastUn provides more consistent estimations of the abundance maps than the compared algorithms.

B. Real data sets

Experiments have been also conducted on two real data sets to empirically assess the performance of the propsoed unmixing method. The first real hyperspectral image is the well-known Cuprite dataset[1]. A subimage of size 250×191 pixels has been used in the experiment. The hyperspectral image is originally composed of 224 bands but the bands 1-2, 105-115, 150-170 and 223-224 have been removed due to poor SNR. The endmember matrix $\mathbf{A}$ has been chosen as a collection of $m = 498$ spectral signatures selected from the spectral library splib06. Since no ground truth abundance maps are associated to this data set, classification map produced by Tetracorder 4.4 [22] have been used as a benchmark. Note that the results in [22] have been only exploited as a proxy of the ground truth, not to design the spectral library $\mathbf{A}$. Fig. 2 shows the estimated abundance map for the Chalcedony mineral. FastUn is shown to provides a consistent map without smoothing the details, contrary to the TV-based methods.

TABLE II
JASPER RIDGE DATA SET: SRE AND SPARSITY LEVELS OBTAINED BY THE COMPARED ALGORITHMS.

	SUnSAL TV	S^{2}WSU	MUA	SUSRLR TV	DRSU TV	RDRSU	FastUn
SRE	8.41	14.00	9.37	9.69	10.67	10.90	**15.15**
sparsity	0.0163	0.0051	0.0184	0.0145	0.0087	0.0078	**0.0051**

Then the compared unmixing algorithms have been used on the Jasper Ridge dataset[2]. The image is composed of 100×100 pixels with 224 spectral bands. Again, the bands numbered 1-3, 108-112, 154-166 and 220-224 have been removed due to poor SNR. Jasper Ridge dataset contains 4 endmembers (tree, water, soil and dirt) and are accompanied with ground truth abundance maps. To evaluate the sparsity of the solutions, the endmember matrix is designed to be made of 498 minerals in addition to the 4 endmembers, i.e., $m = 502$ [23]. The SRE and sparsity levels are reported in Table II. FastUn obtains higher SRE and sparsity values. Moreover, Fig. 3 shows the estimated abundance maps for the tree endmember. The abundance map estimated by FastUn seems to be visually in better agreement with the ground truth than the maps recovered by the compared algorithms.

Finally, the computation times required by all algorithms for the experiments conducted on the simulated and real data sets are reported in Table III. FastUn and MUA are shown to have the smallest computation times compared to other algorithms, which demonstrated the efficiency of the proposed method.

IV. CONCLUSION

This letter proposed a fast sparse unmixing method including a spatial regularization based on superpixel segmentation which allows spatial-spectral information to be extracted, leading to a low-resolution counterpart of the hyperspectral image. A low-resolution abundance map was obtained from this image by solving a weighted ℓ_1-regularized minimization

[1]http://aviris.jpl.nasa.gov/html/aviris.freedata.html

[2]https://rslab.ut.ac.ir/data

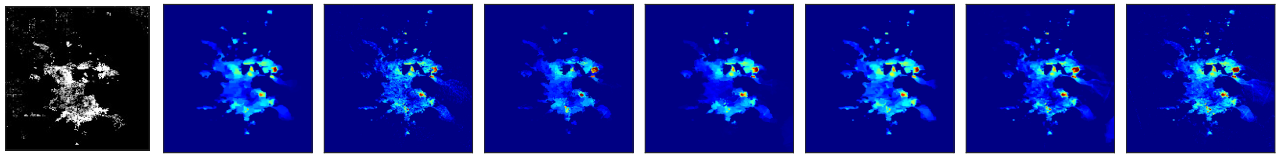

Fig. 2. Cuprite dataset: abundance maps for the chalcedony mineral estimated by the compared algorithms.

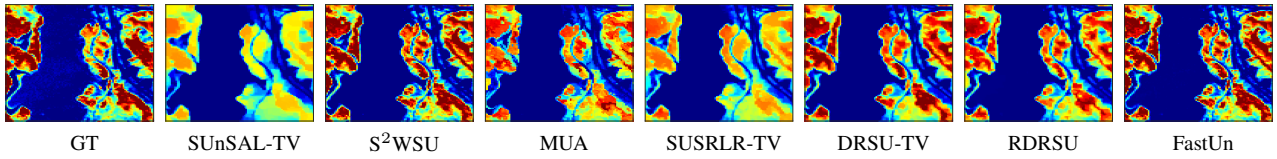

Fig. 3. Jasper Ridge data set: abundance maps for the tree endmember estimated by the compared algorithms.

TABLE III
SIMULATED AND REAL DATA SETS: COMPUTATIONAL TIMES REQUIRED BY THE COMPARED ALGORITHMS.

	SUnSAL TV	**S²WSU**	**MUA**	**SUSRLR TV**	**DRSU TV**	**RDRSU**	**FastUn**
SD1	70.26	24.01	**1.67**	118.19	113.55	107.14	2.82
SD2	97.42	41.07	**7.19**	173.67	166.36	323.85	10.16
Cuprite	1140	384	**113**	1831	1268	1688	138
Jasper Ridge	245	84	93	362	253	367	**35**

problem. This coarse approximation of the abundance map was subsequently used to design a spatially informed regularization that mimicked TV-based regularizations. The high resolution abundance map was finally obtained by solving another weighted ℓ_1-regularized minimization exploited by new spatial regularization. This performance of the resulting FastUn was assessed through experiments conducted on simulated real data sets. It was shown to provide competitive results when compared to state-of-the-art TV-based unmixing algorithms, while coming with a significantly lower computational cost.

REFERENCES

[1] J. M. Bioucas-Dias, A. Plaza, N. Dobigeon, M. Parente, Q. Du, P. Gader, and J. Chanussot, "Hyperspectral unmixing overview: Geometrical, statistical, and sparse regression-based approaches," *IEEE J. Sel. Topics Appl. Earth Observ. Remote Sens.*, vol. 5, no. 2, pp. 354–379, April 2012.

[2] N. Dobigeon, J.-Y. Tourneret, C. Richard, J. C. M. Bermudez, S. McLaughlin, and A. O. Hero, "Nonlinear unmixing of hyperspectral images: Models and algorithms," *IEEE Signal Process. Mag.*, vol. 31, no. 1, pp. 82–94, 2014.

[3] J. S. Bhatt and M. V. Joshi, *Regularization in hyperspectral unmixing*. SPIE, 2016.

[4] V. S S and J. S. Bhatt, "A blind spectral unmixing in wavelet domain," *IEEE J. Sel. Topics Appl. Earth Observ. Remote Sens.*, vol. 14, pp. 10 287–10 302, 2021.

[5] J. M. P. Nascimento and J. M. B. Dias, "Vertex component analysis: a fast algorithm to unmix hyperspectral data," *IEEE Trans. Geosci. Remote Sens.*, vol. 43, no. 4, pp. 898–910, April 2005.

[6] M. E. Winter, "N-findr: An algorithm for fast autonomous spectral endmember determination in hyperspectral data," in *Imaging Spectrometry V*, vol. 3753. International Society for Optics and Photonics, 1999, pp. 266–275.

[7] N. Dobigeon, J. Y. Tourneret, and C. I. Chang, "Semi-supervised linear spectral unmixing using a hierarchical bayesian model for hyperspectral imagery," *IEEE Trans. Signal Process.*, vol. 56, no. 7, pp. 2684–2695, July 2008.

[8] O. Eches, N. Dobigeon, and J. Y. Tourneret, "Enhancing hyperspectral image unmixing with spatial correlations," *IEEE Trans. Geosci. Remote Sens.*, vol. 49, no. 11, pp. 4239–4247, Nov 2011.

[9] M. D. Iordache, J. M. Bioucas-Dias, and A. Plaza, "Total variation spatial regularization for sparse hyperspectral unmixing," *IEEE Trans. Geosci. Remote Sens.*, vol. 50, no. 11, pp. 4484–4502, Nov 2012.

[10] R. Wang, H. Li, A. Pizurica, J. Li, A. Plaza, and W. J. Emery, "Hyperspectral unmixing using double reweighted sparse regression and total variation," *IEEE Geosci. Remote Sens. Lett.*, vol. 14, no. 7, pp. 1146–1150, July 2017.

[11] S. Zhang, J. Li, H. Li, C. Deng, and A. Plaza, "Spectral-spatial weighted sparse regression for hyperspectral image unmixing," *IEEE Trans. Geosci. Remote Sens.*, vol. 56, no. 6, pp. 3265–3276, June 2018.

[12] P. V. Giampouras, K. E. Themelis, A. A. Rontogiannis, and K. D. Koutroumbas, "Simultaneously sparse and low-rank abundance matrix estimation for hyperspectral image unmixing," *IEEE Trans. Geosci. Remote Sens.*, vol. 54, no. 8, pp. 4775–4789, Aug 2016.

[13] J. R. Patel, M. V. Joshi, and J. S. Bhatt, "Abundance estimation using discontinuity preserving and sparsity-induced priors," *IEEE J. Sel. Topics Appl. Earth Observ. Remote Sens.*, vol. 12, no. 7, pp. 2148–2158, 2019.

[14] T. Ince, "Superpixel-based graph Laplacian regularization for sparse hyperspectral unmixing," *IEEE Geosci. Remote Sens. Lett.*, pp. 1–5, 2020.

[15] ——, "Double spatial graph Laplacian regularization for sparse unmixing," *IEEE Geosci. Remote Sens. Lett.*, pp. 1–5, 2021.

[16] R. A. Borsoi, T. Imbiriba, J. C. M. Bermudez, and C. Richard, "A fast multiscale spatial regularization for sparse hyperspectral unmixing," *IEEE Geosci. Remote Sens. Lett.*, vol. 16, no. 4, pp. 598–602, 2019.

[17] H. Li, R. Feng, L. Wang, Y. Zhong, and L. Zhang, "Superpixel-based reweighted low-rank and total variation sparse unmixing for hyperspectral remote sensing imagery," *IEEE Trans. Geosci. Remote Sens.*, pp. 1–19, 2020.

[18] R. Achanta, A. Shaji, K. Smith, A. Lucchi, P. Fua, and S. Süsstrunk, "Slic superpixels compared to state-of-the-art superpixel methods," *IEEE Trans. Pattern Anal. Mach. Intell.*, vol. 34, no. 11, pp. 2274–2282, 2012.

[19] J. M. Bioucas-Dias and M. A. T. Figueiredo, "Alternating direction algorithms for constrained sparse regression: Application to hyperspectral unmixing," in *Proc. 2nd Workshop Hyperspectral Image Signal Process., Evol. Remote Sens. (WHISPERS)*, June 2010, pp. 1–4.

[20] F. Li, S. Zhang, C. Deng, B. Liang, J. Cao, and S. Wang, "Robust double spatial regularization sparse hyperspectral unmixing," *IEEE J. Sel. Topics Appl. Earth Observ. Remote Sens.*, vol. 14, pp. 12 569–12 582, 2021.

[21] R. N. Clark *et al.*, *USGS digital spectral library splib06a*. U.S. Geological Survey Denver, CO, 2007.

[22] ——, "Imaging spectroscopy: Earth and planetary remote sensing with the USGS Tetracorder and expert systems," *J. Geophys. Res.*, vol. 108, no. E12, p. 5131, Dec. 2003.

[23] L. Qi, J. Li, Y. Wang, Y. Huang, and X. Gao, "Spectral-spatial-weighted multiview collaborative sparse unmixing for hyperspectral images," *IEEE Trans. Geosci. Remote Sens.*, vol. 58, no. 12, pp. 8766–8779, 2020.